Soft Matter

Crystallization at Droplet Interfaces for the Fabrication of Geometrically Programmed Synthetic Magnetosomes

Journal:	*Soft Matter*
Manuscript ID	SM-ART-03-2020-000410.R1
Article Type:	Paper
Date Submitted by the Author:	08-Apr-2020
Complete List of Authors:	Stoller, Michael; University of Nebraska - Lincoln, Chemistry Gromowsky, Matthew; University of Nebraska - Lincoln, Chemistry Rauhauser, Maddee; University of Nebraska - Lincoln, Chemistry Judah, Marcus; University of Nebraska - Lincoln, Chemistry Konda, Abhiteja; University of Nebraska - Lincoln, Chemistry Jurich, Christopher; University of Nebraska - Lincoln, Chemistry Morin, Stephen; University of Nebraska - Lincoln, Chemistry

ARTICLE

Crystallization at Droplet Interfaces for the Fabrication of Geometrically Programmed Synthetic Magnetosomes

Received 00th January 20xx,
Accepted 00th January 20xx

DOI: 10.1039/x0xx00000x

Michael A. Stoller,[a] Matthew Gromowsky,[a] Maddee Rauhauser,[a] Marcus Judah,[a] Abhiteja Konda,[a] Chris Jurich,[a] Stephen A. Morin[ab†]

Biological systems demonstrate exquisite three dimensional (3D) control over crystal nucleation and growth using soft micro/nanoenvironments, such as vesicles, for reagent transport and confinement. It remains challenging to mimic such biomineralization processes using synthetic systems. A sythetic mineralization strategy applicable to the synthesis of artificial magnetosomes with programmable magnetic domains is described. This strategy relies on the compartmentalization of precursors in surfactant-stabilized liquid microdroplets which, when contacted, spontaneously form lipid bilayers that support reagent transport and interface-confined magnetite nucleation and growth. The resulting magnetic domains are polarized and thus readily manipulated using magnetic fields or assembled using droplet-droplet interactions. This strategy presents a new, liquid phase procedure for the synthesis of vesicles with geometrically controlled inorganic features that would be difficult to produce otherwise. The artificial magnetosomes demonstrated could find use in, for example, drug/cargo delivery, droplet microfluidics, and formulation science.

Introduction

In biomineralization organic/inorganic materials are combined in sophisticated architectures that provide critical functionality (e.g., the structural rigidity of skeletal systems and the directional sensing capabilities of magnetotactic bacteria).[1] Mimicking the spatial control of crystal nucleation/growth found in biomineralization, synthetically, remains a significant challenge due to the complexities associated with compartmentalizing, transporting, and mixing inorganic precursors in 3D micro/nanoenvironments.[2] Methods that combine synthetic vesicles (surfactant-stabilized droplets) and microfluidics for the compartmentalization and transport of inorganic precursors could address these limitations and thus enable the rational nucleation and growth of functional materials in processes more like those found in biology.

To demonstrate this concept, we synthesized magnetic particles at droplet interface bilayers (DIBs)[3] for the bottom-up production of hybrid structures with programmed geometry and functionality. Specifically, we produce precursor-loaded, water-in-oil microdroplets using asolectin as a surfactant and standard microfluidic procedures. When the microdroplets were brought into contact with one another, a DIB was spontaneously formed, and diffusion-based transport of precursors across the interface initiated localized mineralization. This process could be tuned by controlling the precursor species and concentration in the microdroplets. We used this approach to produce a variety of "synthetic magnetosomes"[4] (SMs) with rationally controlled magnetic domains.

In addition to controlling the location of the magnetic domains, it was also possible to manipulate these domains during growth using external magnetic fields. This property enabled the generation of "chiral" filaments and the formation of droplets with different magnetic polarity. Furthermore, the polarized magnetic domains of the SMs could be used to drive their assembly into elongated structures.

The approach we report relies on precursor compartmentalization and transport using surfactant-stabilized microdroplets and simple microfluidic devices, respectively, thus enabling the programmed synthesis of SMs using scalable liquid-based processing techniques. This procedure is generalizable to other materials with different functional properties (e.g., semiconducting and catalytic microparticles). Further, the concept of droplet-interface-confined nucleation/growth of functional materials provides access to a new class of soft/hard hybrid materials with synthetic programmability that mimics characteristics of biomineralization. These findings are potentially useful to scientists studying ferrofluids,[5] drug/cargo transprot,[6] magnetic resonance imaging (MRI) contrast agents,[7–12] formulation science,[13] and cancer thereputics.[14]

We began by considering the methods available to generate synthetic vesicles with tunable transport properties. Ubiquitous in nature, lipid bilayers are essential to the structure and function of vesicles and, more generally, cells. There have been

[a] Dept. of Chemistry, University of Nebraska–Lincoln, Hamilton Hall, Lincoln, NE 68588.
[b] Nebraska Center for Materials and Nanoscience, University of Nebraska–Lincoln, Lincoln, NE 68588.Address here.
† To whom correspondence should be addressed. Telephone: (402) 472-4608. Fax: (402) 472-9402. E-mail: smorin2@unl.edu.
Electronic Supplementary Information (ESI) available: [details of any supplementary information available should be included here]. See DOI: 10.1039/x0xx00000x

many technological advancements that have enabled the study of biologically relevant lipid bilayers synthetically and that do not require the use of live cells. So called "artificial" lipid bilayers, which are constructed using biologically and synthetically derived phospholipids, are used to study the effects of lipid chemistry on the passive transport properties of lipid bilayers, active transport function of trans-membrane proteins, and architecture of lipid bilayers systematically.[15]

Planar versions of artificial lipid bilayers used in such studies (e.g., the investigation of membrane proteins within bilayers supported on micromachined substrates)[16–19] are commonly produced using the Montal-Muller method.[20,21] The bilayers formed using the Montal-Muller method are, however, metastable, and thus have limited application to conventional analytical protocols and in microfluidic devices.[20,21] In contrast, lipid bilayers produced following DIB procedures have exceptional stability, with lifetimes of days to weeks (compared to a few hours with the Montal-Muller approach).[22–25] In the DIB method, bilayers are produced by contacting aqueous microdroplets formed in oil-lipid mixtures. These aqueous microdroplets are coated with self-assembled lipid monolayers that, when brought into contact, spontaneously form a lipid bilayer as oil is displaced from the contact interface. Two procedures are followed to produce DIBs: the "lipid in" method uses lipid vesicles dispersed within the aqueous phase and the "lipid out" method uses lipids dissolved in the oil phase.[23,26] For maximum effectiveness in DIB formation, a prescribed stabilization period should be allowed following introduction of the aqueous phase in to the oil or lipid-oil mixture so that the required lipid monolayers can form.[27]

Osmosis across DIBs has been used to modulate supersaturation within droplets, providing a biomimetic approach to control the nucleation/growth of inorganic crystals in confined volumes.[28] In the present work we demonstrate, for the first time, the transport of precursor species across DIBs for the controlled initiation of precipitation reactions and thus the localized growth of desired inorganic materials at the interface of droplets.

A prototypical biomineral formed within cellular vesicles (i.e., liquids enclosed by lipid bilayers) is magnetite (Fe_3O_4), a magnetic iron oxide. For example, magnetotactic bacteria use vesicle-enclosed magnetite particles ("magnetosomes") to orient their bodies relative to the magnetic field of Earth. Magnetosomes contain crystals of magnetite that range in size from 30 to 120 nm. In this size regime each crystal contains a single magnetic domain that drives crystal alignment and the spontaneous polarization of the magnetosomes (smaller crystals are superparamagnetic while larger crystals contain multiple magnetic domains).[29] Synthetic magnetite particles have broad applicability in, for example, nano/biotechnologies,[30] data recording,[31] medical therapeutics (drug delivery,)[6,32] cancer treatment,[5,14] ferrofluids,[33] biomolecular scavenging,[34] and adaptive inks.[35]

Experimental Design

Due to the broad range of applications of synthetic magnetite and its convenient synthesis under room temperature, aqueous conditions, we focused this study on the growth of magnetite at DIBs enabling the design and synthesis of artificial magnetosomes with programmable magnetic features. In this system, we have control over the location of magnetite precipitation, its polarization, and (because we can tune the supersaturation of the system) the size of the crystals. We used hexadecane as a continuous phase and asolectin as a surfactant for aqueous droplets as this is a well-established droplet system in literature.[36,37] Ammonia (from ammonium hydroxide) was used to generate hydroxide because ammonia is a small, uncharged species that can readily diffuse across lipid bilayers. Iron(II) chloride and iron(III) chloride were used as precursors for magnetite growth following well-established protocols.[38]

We used 3D printing, soft lithography, and surface passivation chemistry to prototype microfluidic droplet generators and reaction wells (see supporting information). This approach facilitated containment, manipulation, and imaging of single/multiple droplets simultaneously, dramatically increasing throughput of the described experiments. We demonstrated the ability to produce magnetosomes with single/multiple magnetic domains in predetermined positions. This capability allows for the synthesis of magnetosomes which orient/move uniquely within magnetic fields.

Results & Discussion

We hypothesized that rapid crystal nucleation/growth at DIBs could be used to suppress reagent transport into a droplet, and thus concentrate the formation of crystals to the DIB site while limiting the formation of crystals within the internal volume of a droplet (Fig. 1A). To test this hypothesis, we synthesized phospholipid stabilized microdroplets containing $FeCl_2$ and $FeCl_3$ or NH_3 (Fig. 1A,B). When contacted these droplets spontaneously form a DIB (Fig. 1B,C) and transport between droplets initiates nucleation/growth (Fig. 1B-D). As has been demonstrated,[39] small uncharged molecules (e.g., NH_3 and H_2O) can move between droplets, through the DIB, along gradients in concentration and ionic strength while charged species (e.g., Cl^-, Fe^{2+}, Fe^{3+}) do not cross the DIB (Fig. 1B).

To confirm the transport of ammonia across the DIB, we contacted a droplet containing ammonium hydroxide with one containing cobalt (II) chloride. As shown here and elsewhere, aqueous $Co(NH_3)_x^{2+}$ complexes are colored and their formation is readily identified visually (or spectroscopically). Thus, a color change in the Co^{2+} upon contact with the ammonium hydroxide droplet indicated NH_3 transport across the DIB (Fig. S1). We further confirmed the transport of ammonium using an acid/base indicator (phenolphthalein) (Fig. S2).

In a typical mineralization experiment, we contacted droplets containing iron(II) and iron(III) (in a 1:2 ratio) with droplets containing ammonium hydroxide. NH_3 transport into the $Fe^{2+/3+}$ droplet initiated the room temperature synthesis of magnetite via the Schikorr reaction:[40]

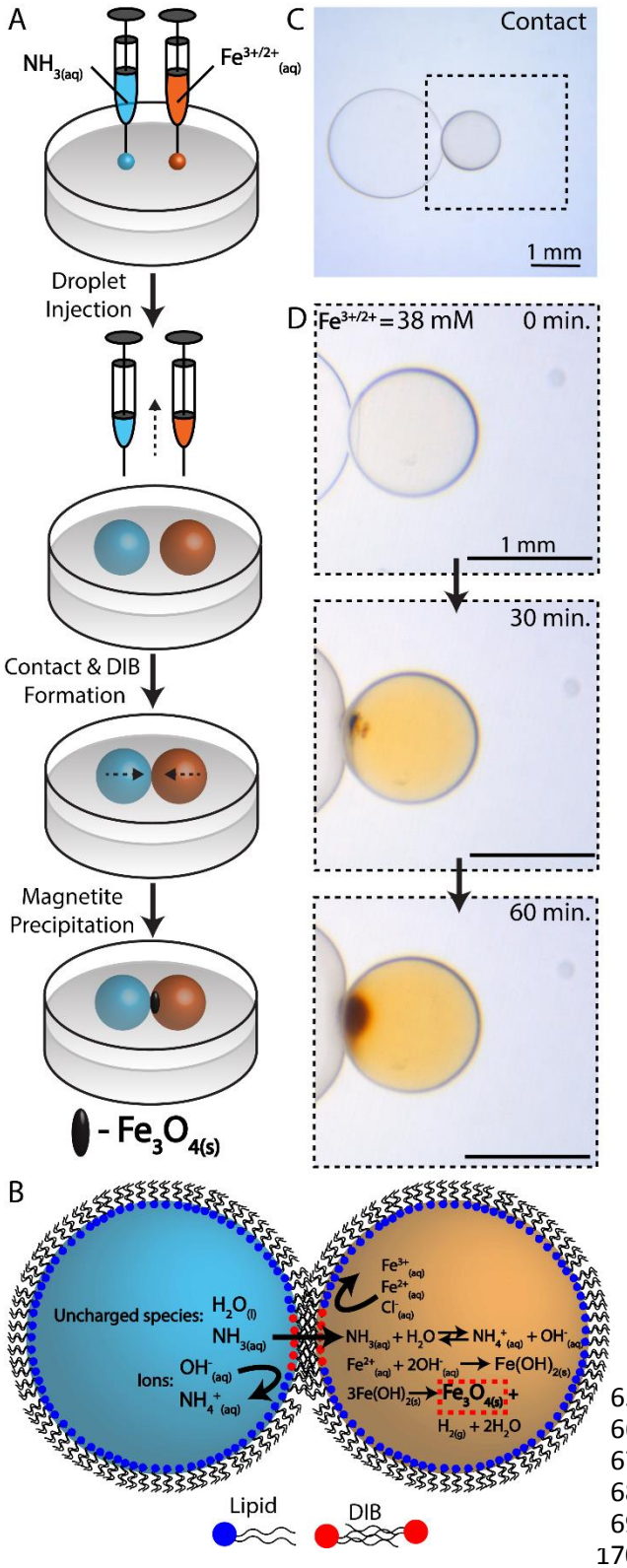

Fig. 1. Synthesis of synthetic magnetosomes (SMs). (A) Schematic illustration of the synthetic procedure where two precursor droplets are contacted to initiate interface-confined growth of magnetite. (B) Schematic detailing the transport and chemical processes that occur in DIB magnetite synthesis. (C) Image of DIB formation on first contact of two droplets. (D) Image sequence showing the growth of magnetite over time.

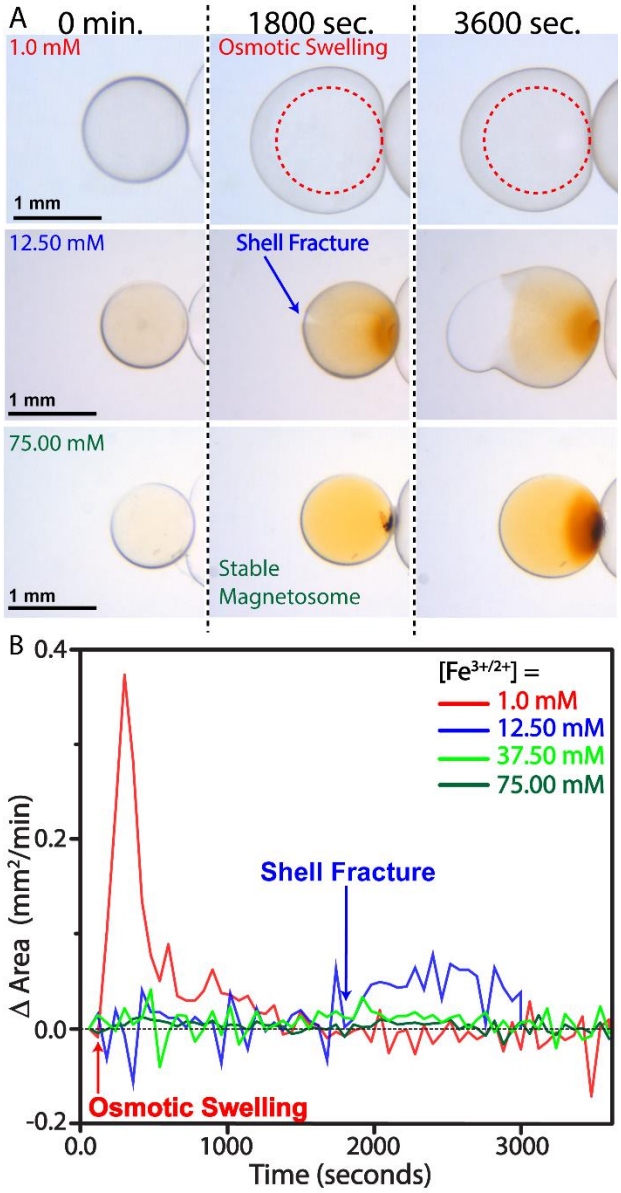

Fig. 2. Effect of precursor concentration on SM growth. (A) Growth over time for three iron precursor concentrations. Row 1: No iron oxide shell forms and growth via osmotic swelling; Row 2: Iron oxide shell is fractured by osmotic pressure; Row 3: Stable SM is formed. (B) Temporal traces show change in droplet area for droplets in the three regimes.

$$3Fe(OH)_2 \rightarrow Fe_3O_4 + H_2 + 2H_2O.$$

We confirmed the product of this reaction to be magnetite using selected area electron diffraction (SAED) (Fig. S3 and S4). The simulation and analysis of the SAED pattern was carried out with Landyne 3 software.[41]

We observed a strong dependence of the growth behavior on the concentration of the iron precursors in the target droplet (where magnetite forms) (Fig. 2). Specifically, we observed three different growth behaviors: (i) At very low iron concentration, there is no visible color change, and we

concluded there was thus very little if any magnetite growth (in this regime the iron-containing droplet increased in volume due to osmosis) (Fig. 2A top row); (ii) At 12.5 mM $Fe^{2+/3+}$, a rigid shell forms along the interior of the droplet. This shell could form due to preferential nucleation/growth of magnetite at the lipid interface or through the formation of interfacial complexes between the phospholipid and soluble/insoluble iron oxide species. Regardless, in this concentration regime, the target droplet maintains a constant volume until eventually the shell cracks (presumably due to osmotic pressure) (Fig. 2A middle row); (iii) At the highest $Fe^{2+/3+}$ concentrations we observe magnetite growth that was mostly confined to the DIB contact zone (Fig. 2A bottom row).

Ammonia transport across the DIB was driven by: (i) the initial concentration gradient across the DIB set by the given experimental conditions and (ii) Le Chatelier's principle which dictates that the consumption of OH^- in the Shikorr reaction will continuously drive the conversion of ammonia to ammonium until the $Fe^{2+/3+}$ was consumed, thus maintaining a concentration gradient that drives ammonia transport until precipitation is complete. The existence of a gradient in ionic strength across the DIB (favoring the $Fe^{2+/3+}$ droplet) coupled with the formation of a magnetite shell on the $Fe^{2+/3+}$ droplet develops osmotic pressure. If the shell thickness is adequate to contain this pressure, the magnetosome is stable and the droplet does not rupture (or grow in volume) (Fig. 2A bottom row and Fig. 2B).

We could manipulate the magnetite during mineralization using magnetic fields. In a simple demonstration of this capability we placed a magnet ~1 cm from the DIB interface during mineralization, “pulling” a fibril-like magnetite column toward the magnet and rotating the target droplet during the process (Figure 3 and Videos S1-S2). This procedure was directional and could potentially be used to develop magnetosomes with “chiral” magnetite morphologies. We believe that translocation of the magnetite-“clogged” interface toward the magnet generated clear DIB that was critical for fast diffusion and continued growth.

We show that by positioning ammonia-loaded droplets to contact $Fe^{2+/3+}$ droplets, thus forming DIBs at defined positions around the target droplet, we can produce artificial magnetosomes with asymmetric or symmetric magnetic domains (Fig. 4A-F). This utility can be used to tune the response of these magnetosomes to magnetic fields (e.g., their field-induced movements). As examples of this utility, we showed that an asymmetrically loaded droplet moves through a liquid (the continuous phase, hexadecane) toward a nearby magnet (Fig. 4E and Video S3). Similarly, magnetosomes produced in this manner will match the clockwise/counterclockwise rotation of a rotating magnetic field generated by a stir plate (Fig. S5 and Video S4). Throughout these manipulations the magnetic domains of the SMs remained in place, and did not translocate relative to one another, supporting the assertion that the mineralized interfaces of the SMs are solid.

To investigate the polarity of the as-synthesized magnetic domains, we placed SMs with a single domain in a rotating magnetic field (Video S5-S9). We observed that the droplets are

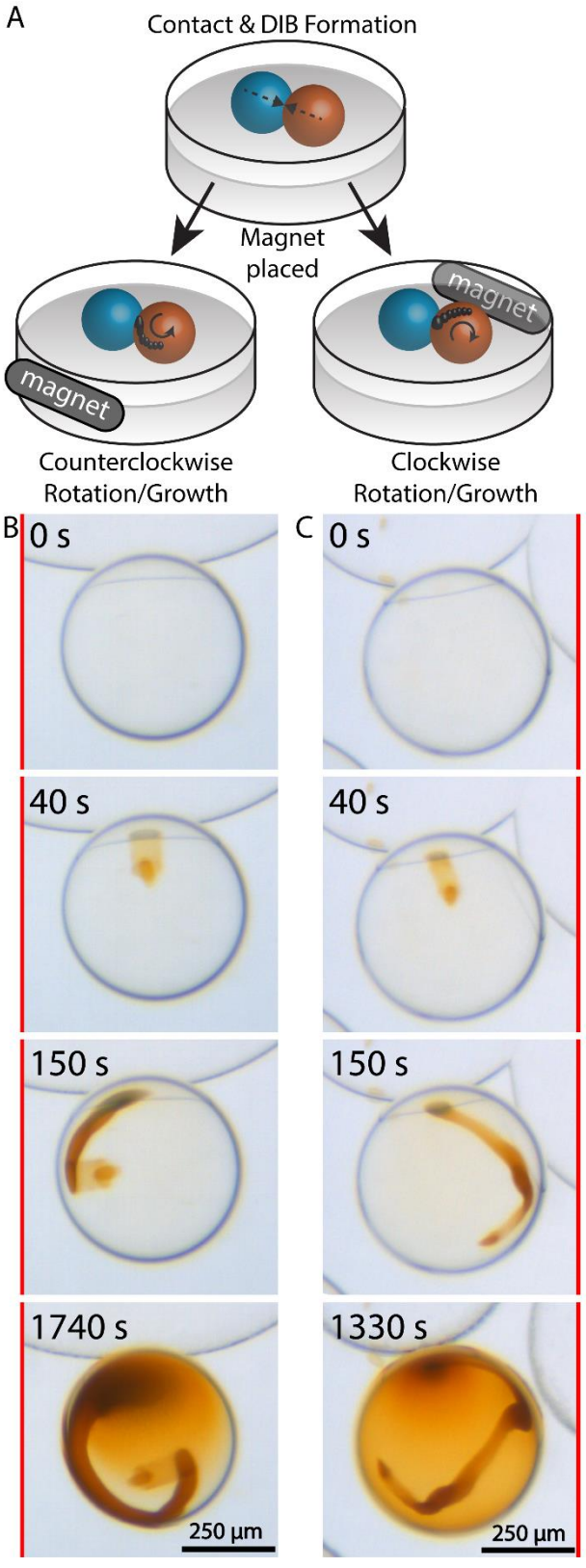

Fig. 3. Manipulation of SM growth using magnetic fields. (A) Schematic illustration showing the influence of a magnet on magnetite growth. (B) Image sequence showing the growth of iron oxide with a magnet to the left (annotated with red line). (C) Image sequence showing the growth of iron oxide with a magnet to the right (annotated with red line).

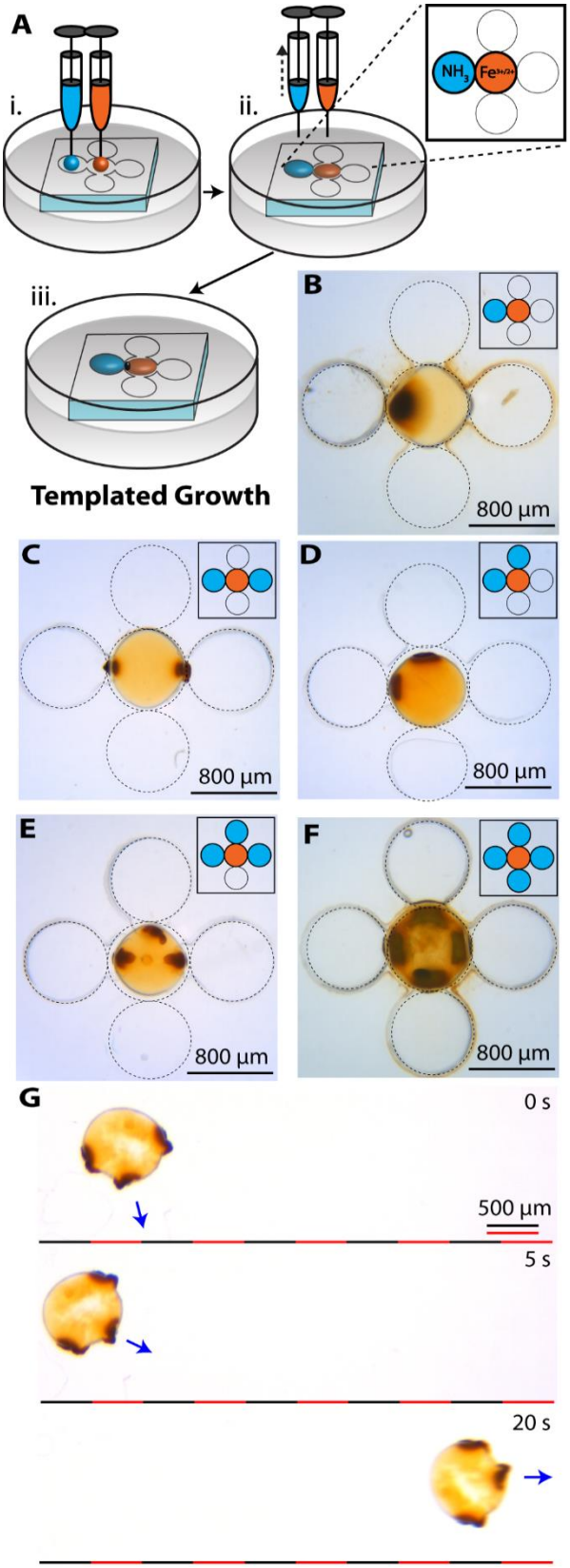

Fig. 4. Multi-domain SMs. (A) Schematic illustrating the loading of droplets into PDMS templates to form DIBs at controlled locations. (B-F) Schematics and representative images of different varieties of single/multi-domain SMs. (G) image sequence showing the reorientation and movement of a multi-domain SM from panel E in response to an external magnetic field.

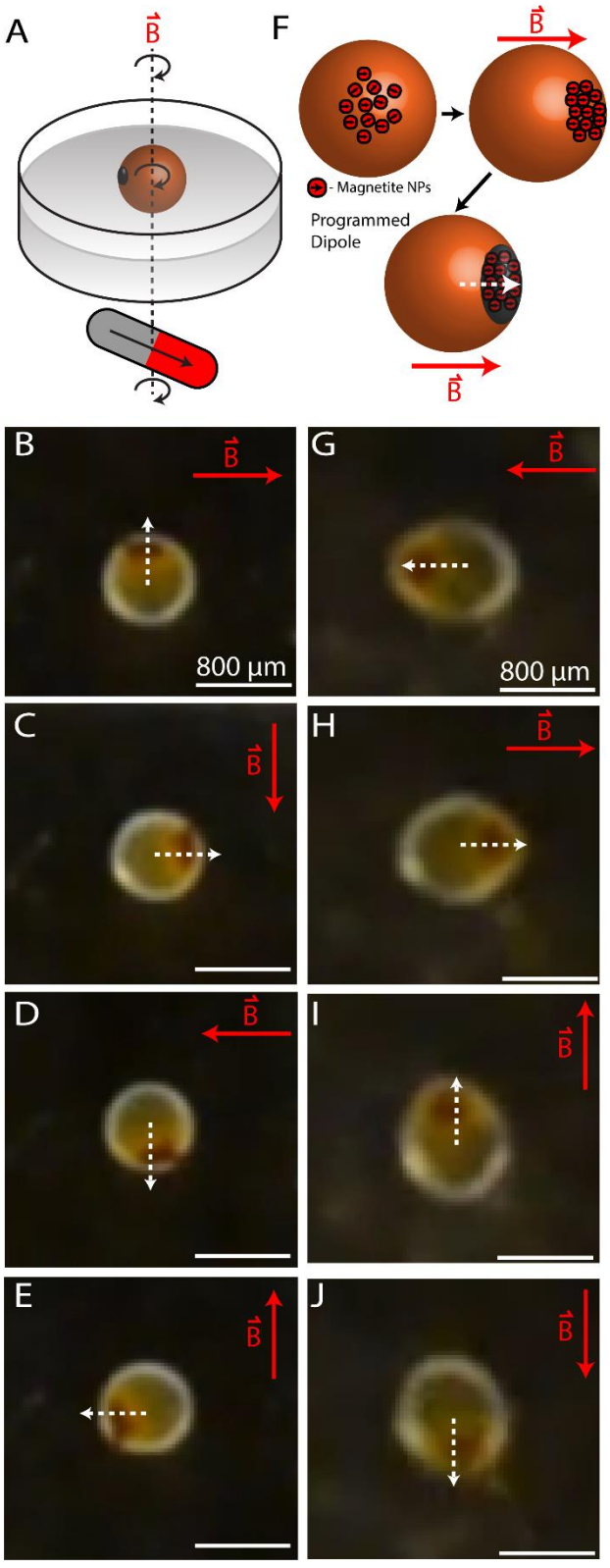

Fig. 5. Polarization of SMs. Schematic (A) and image sequence (B-E) showing the orientation of a single domain SM (synthesized in the absence of a magnetic field) rotating in a magnetic field. (F) Schematic illustration of the procedure used to program the polarization of an SM arbitrarily. (G-J) Image sequence showing rotation of a programmed single domain SM in an external magnetic field. Note vector from center of SM to magnetic domain aligns with the magnetic field vector B.

234 polarized perpendicular to a line drawn from the center of the

droplet to the magnetic domain (Fig. 5A-E). We hypothesize that during growth magnetite particles adopt a distribution of alignment that favors polarization along the edge of the droplet because this alignment distribution maximizes surface/magnetic interactions, thus giving rise to a net magnetic dipole in each magnetic domain. To overcome (control) the preferred orientation of the magnetic domains, we employed a magnetic field "templated" approach where pre-synthesized magnetite particles were loaded into a droplet along with $Fe^{2+/3+}$ precursor. A magnetic field was applied to concentrate and orient the particles in the preferred location and an ammonium hydroxide droplet was introduced to form a DIB and initiate magnetite growth. This particle overgrowth "locks" the polarity of the magnetic domain formed (Fig. 5F-J and Video S10).

The serial, drop-by-drop fabrication method utilized to this point could be problematic to scalability. To address this issue, we developed a parallel fabrication procedure that is applicable to the fabrication of hundreds to thousands of monodispersed SMs, simultaneously (Fig.6A-D). As before, these SMs are easily manipulated using a magnet, a procedure useful to collection of products (Video S11).

This approach presented the opportunity to observe the self-assembly of many droplets at once—a phenomena that was anticipated based upon the polarization of the individual magnetic domains. The interactions were apparent from the formation of dimers, trimers, etc. that can be categorized as follows: parallel (P), parallel skewed (PS), antiparallel (AP), head-to-tail (HT), head-to-head (HH), tail-to-tail (TT) or unaligned (U) (Fig. 6C,E). Observation of many (N=1,064) droplets gave the following population distribution: 46.8 % U and 26.3 % P or PS (Fig. 6E). We calculated the population distribution expected based on random probability (which would be the case when magnetic interactions were absent) and would expect the following distribution: 74.3 % U and 9.02 % P or PS (Fig. 6E and Fig. S6). The observed P and PS alignment occurred at a rate that was ~3X than that expected from random interactions. We attribute this observed self-assembling property to the magnetic polarization along the edge of the magnetic domains (Fig. 6E).

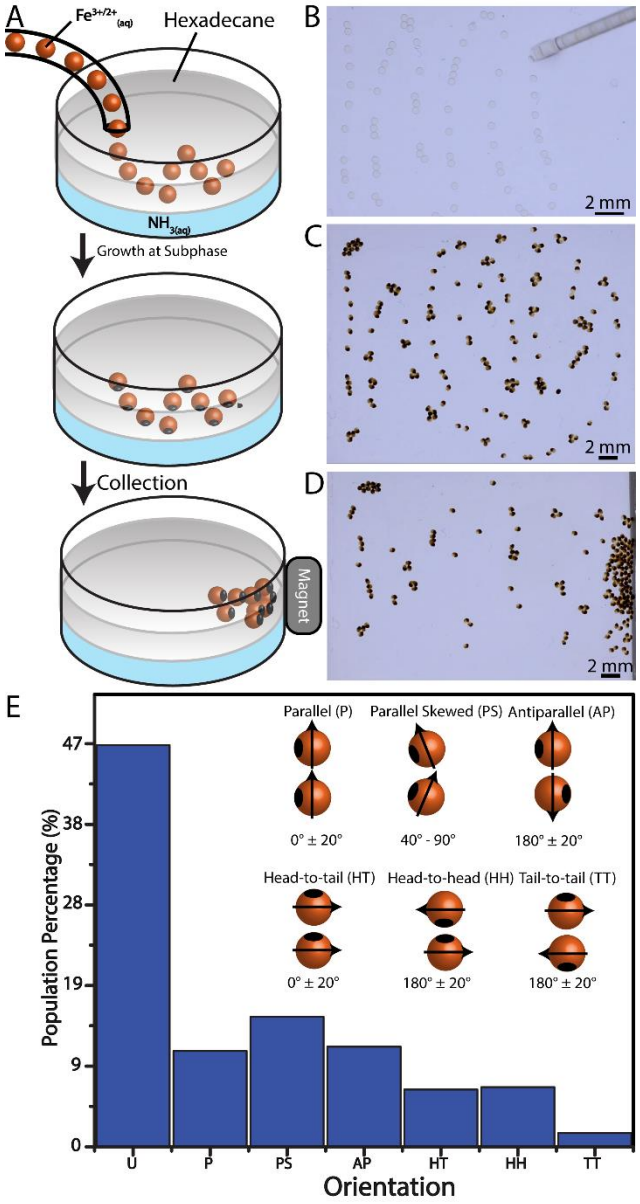

Fig. 6. Parallel synthesis of SMs using microfluidics. (A) Schematic illustration of Fe2+/3+ microdroplets injected into a hexadecane continuous phase with an NH_3 subphase. Magnetite synthesis begins at subphase/microdroplet interface and the resulting SMs are collected with a magnet. (B-D) Corresponding images of the SMs synthesized as shown in panel A. (E) Orientation distribution of a population (N = 1,064) of SM dimers, trimers, etc.

Conclusions

We combine passive transport, aqueous mineralization procedures, and microfluidics to produce synthetic magnetosomes with programed magnetic domains. This approach to the production of rigid, magnetic features on the surface of surfactant stabilized droplets under ambient conditions mimics the production of inorganic/organic hybrid materials seen in biomineralization. The distribution of alignments of individual magnetite particles favor polarization of individual droplets along the droplet edge and lead to droplet-droplet alignment via magnetic effects. This method could be used to develop synthetic procedures to produce inorganic materials that are biologically compatible. This approach provides opportunities to tune crystal growth by changing the lipids used, thereby altering the rate of diffusion and deliver of precursor species; additionally, transmembrane pore forming proteins like alpha-hemolysin can be incorporated to further control the transport properties of DIBs for mineralization control.[42,43]

This approach to crystal growth is simple to perform, requires readily available reagents, takes place at ambient conditions, and is easily monitored/controlled using microfluidic devices and optical microscopy. Researchers interested in the biomimetic fabrication of materials with properties related to magnetic bacteria could employ the reported procedures in materials design/production. Scientists studying ferrofluids,[5] magnetic microswimmers,[44,45] drug/cargo

delivery,[6] droplet microfluidics,[36,37] magnetic resonance imaging,[7–12] formulation science,[13] and magnetic particle hyperthermia tumor therapy[14] may benefit from the general strategies reported.

Conflicts of interest

There are no conflicts to declare

Acknowledgements

This work was supported by the National Science Foundation under Grant no. 1555356. We thank the Department of Chemistry and the Nebraska Center for Materials and Nano Science (NCMN) at the University of Nebraska–Lincoln for start-up funds. S.A.M. thanks 3M for support through a Non-Tenured Faculty Award. The research was performed in part in the Nebraska Nanoscale Facility: National Nanotechnology Coordinated Infrastructure and the Nebraska Center for Materials and Nanoscience (and/or NERCF), which are supported by the National Science Foundation under Award ECCS: 1542182, and the Nebraska Research Initiative. We thank Dr. Xing-Zhong Li (at NCMN) for providing Landyne software and for his support on TEM work.

Notes and references

1 R. Blakemore, *Science*, 1975, **190**, 377–379.
2 S. A. Hutchens, R. S. Benson, B. R. Evans, H. M. O'Neill and J. Rawn, *Biomaterials*, 2006, **27**, 4661–4670.
3 H. Bayley, B. Cronin, A. Heron, M. A. Holden, W. L. Hwang, R. Syeda, J. Thompson and M. Wallace, *Mol. Biosyst.*, 2008, **4**, 1191–1208.
4 P. K. Bakhshi, J. Bain, M. O. Gul, E. Stride, M. Edirisinghe and S. S. Staniland, *Macromol. Biosci.*, 2016, **16**, 1555–1561.
5 C. Alexiou, R. J. Schmid, R. Jurgons, M. Kremer, G. Wanner, C. Bergemann, E. Huenges, T. Nawroth, W. Arnold and F. G. Parak, *Eur. Biophys. J.*, 2006, **35**, 446–450.
6 T. K. Jain, M. A. Morales, S. K. Sahoo, D. L. Leslie-Pelecky and V. Labhasetwar, *Mol. Pharm.*, 2005, **2**, 194–205.
7 J. W. M. Bulte, in *Magnetic Resonance Imaging*, 2006, pp. 419–439.
8 M. Modo, M. Hoehn and J. W. M. Bulte, *Mol. Imaging*, 2005, **4**, 143–164.
9 S. Laurent, D. Forge, M. Port, A. Roch, C. Robic, L. Vander Elst and R. N. Muller, *Chem. Rev.*, 2008, **108**, 2064–2110.
10 S. Boutry, S. Laurent, L. Vander Elst and R. N. Muller, *Contrast Media Mol. Imaging*, 2006, **1**, 15–22.
11 L. Babes, B. Denizot, G. Tanguy, J. J. Le Jeune and P. Jallet, *Colloid Interface Sci.*, 1999, **212**, 474–482.
12 C. Corot, P. Robert, J. M. Idée and M. Port, *Adv. Drug Deliv. Rev.*, 2006, **58**, 1471–1504.
13 R. A. Revia and M. Zhang, *Mater. Today*, 2016, **19**, 157–168.
14 A. J. Giustini, A. A. Petryk, S. M. Cassim, J. A. Tate, I. Baker and P. J. Hoopes, *Nano Life*, , DOI:10.1142/S1793984410000067.
15 S. Kawato, K. Kinosita and A. Ikegami, *Biochemistry*, 1977, **16**, 2319–2324.
16 C. Schmidt, M. Mayer and H. Vogel, *Angew. Chemie - Int. Ed.*, 2000, **39**, 3137–3140.
17 H.-J. Neubert, *Anal. Chem.*, 2008, **76**, 327 A-330A.
18 N. Fertig, A. Tilke, R. H. Blick, J. P. Kotthaus, J. C. Behrends and G. Ten Bruggencate, *Appl. Phys. Lett.*, 2000, **77**, 1218–1220.
19 X. Li, K. G. Klemic, M. A. Reed and F. J. Sigworth, *Nano Lett.*, 2006, **6**, 815–819.
20 M. Montal and P. Mueller, *Proc. Natl. Acad. Sci. U. S. A.*, 1972, **69**, 3561–3566.
21 P. Mueller, D. O. Rudin, H. Ti Tien and W. C. Wescott, *Nature*, 1962, **194**, 979–980.
22 S. H. White, *Biophys. J.*, 1972, **12**, 432–445.
23 W. L. Hwang, M. A. Holden, S. White and H. Bayley, *J. Am. Chem. Soc.*, 2007, **129**, 11854–11864.
24 M. A. Holden, D. Needham and H. Bayley, *J. Am. Chem. Soc.*, 2007, **129**, 8650–8655.
25 J. R. Thompson, A. J. Heron, Y. Santoso and M. I. Wallace, *Nano Lett.*, 2007, **7**, 3875–3878.
26 K. Funakoshi, H. Suzuki and S. Takeuchi, *Anal. Chem.*, 2006, **78**, 8169–8174.
27 D. J. Mitev, T. Ivanova and C. S. Vassilieff, *Colloids Surfaces B Biointerfaces*, 2002, **24**, 185–192.
28 Z. Michalak, D. Fartash, N. Haque and S. Lee, *CrystEngComm*, 2012, **14**, 7865–7868.
29 D. Faivre, A. Fischer, I. Garcia-Rubio, G. Mastrogiacomo and A. U. Gehring, *Biophys. J.*, 2010, **99**, 1268–1273.
30 R. M. Cornell and U. Schwertmann, *The iron oxides: structure, properties, reactions, occurrences and uses: second ed.*, 2003.
31 S. Sun, C. B. Murray, D. Weller, L. Folks and A. Moser, *Science (80-.).*, 2000, **287**, 1989–1992.
32 I. Chourpa, L. Douziech-Eyrolles, L. Ngaboni-Okassa, J. F. Fouquenet, S. Cohen-Jonathan, M. Soucé, H. Marchais and P. Dubois, *Analyst*, , DOI:10.1039/b419004a.
33 E. H. Kim, H. S. Lee, B. K. Kwak and B. K. Kim, in *Journal of Magnetism and Magnetic Materials*, 2005.
34 C. Lang, D. Schüler and D. Faivre, *Macromol. Biosci.*, 2007, **7**, 144–151.
35 S. W. Charles and J. Popplewell, *Endeavour*, 1982, **6**, 153–161.
36 M. Zagnoni and J. M. Cooper, *Lab Chip*, 2010, **10**, 3069–3073.
37 B. Schlicht and M. Zagnoni, *Sci. Rep.*, 2015, **5**, 1–8.
38 L. Vayssières, C. Chanéac, E. Tronc and J. P. Jolivet, *J. Colloid Interface Sci.*, 1998, **205**, 205–212.
39 J. Berg, J. Tymoczko and L. Stryer, *Biochemistry, 5th edition*, 2002.
40 G. Schikorr, *Zeitschrift für Anorg. und Allg. Chemie*, 1933, **212**, 33–39.
41 X.-Z. Li, *Microsc. Microanal.*, 2016, **22**, 564–565.
42 E. J. Challita, J. S. Najem, R. Monroe, D. J. Leo and E. C. Freeman, *Sci. Rep.*, 2018, **8**, 1–11.
43 S. Leptihn, O. K. Castell, B. Cronin, E. H. Lee, L. C. M. Gross, D. P. Marshall, J. R. Thompson, M. Holden and M. I. Wallace,

Nat. Protoc., 2013, **8**, 1048–1057.

44 A. W. Mahoney, J. C. Sarrazin, E. Bamberg and J. J. Abbott, *Adv. Robot.*, , DOI:10.1163/016918611X568620.

45 K. Bente, A. Codutti, F. Bachmann and D. Faivre, *Small*, 2018, **14**, 1704374.

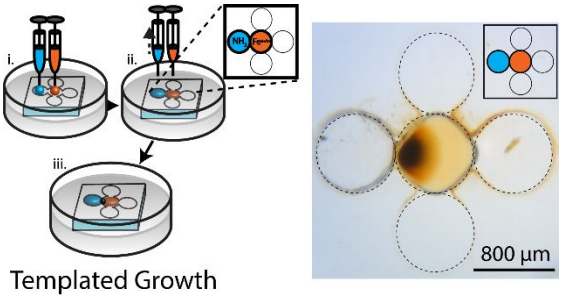

A synthetic mineralization strategy applicable to the synthesis of artificial magnetosomes with programmable magnetic domains is described. The resulting magnetic domains are polarized and thus readily manipulated using magnetic fields or assembled using droplet-droplet interactions